2024 IEEE International Conference on Robotics and Automation (ICRA 2024)
May 13-17, 2024. Yokohama, Japan

SATac: A Thermoluminescence Enabled Tactile Sensor for Concurrent Perception of Temperature, Pressure, and Shear

Ziwu Song*, Ran Yu*, Xuan Zhang, Kit Wa Sou, Shilong Mu, Dengfeng Peng, Xiao-Ping Zhang, *Fellow, IEEE*, Wenbo Ding

***Abstract*— Most vision-based tactile sensors use elastomer deformation to infer tactile information, which can not sense some modalities, like temperature. As an important part of human tactile perception, temperature sensing can help robots better interact with the environment. In this work, we propose a novel multi-modal vision-based tactile sensor, SATac, which can simultaneously perceive information on temperature, pressure, and shear. SATac utilizes the thermoluminescence of strontium aluminate to sense a wide range of temperatures with exceptional resolution. Additionally, the pressure and shear can also be perceived by analyzing the Voronoi diagram. A series of experiments are conducted to verify the performance of our proposed sensor. We also discuss the possible application scenarios and demonstrate how SATac could benefit robot perception capabilities.**

I. Introduction

In the realm of robotic tactile perception, the pursuit of equipping robots with tactile sensing capabilities that match or even surpass human proficiency is deemed pivotal. Such advancements can significantly enhance a robot's ability to execute intricate tasks, ranging from grasping and object recognition to dexterous manipulation [1]–[3].

Solutions for achieving robotic tactile sensing can be broadly categorized into two main types: electrical signal-based approach [4] and vision-based approach [5]. The former boasts a more extensive historical foundation and is renowned for its high sensing precision. However, with the growing demand for dexterous robotic manipulation [6]–[8], the significance of high spatial resolution sensing has become evident [9]. The vision-based approach emerges as a more competitive solution with both cost-effectiveness and robustness while ensuring real-time sampling rates, superior resolution, and an extensive sensing range [10]–[13]. These advantages have positioned it as the focal point of robotic sensing research. Vision-based tactile sensors like GelSight [5], GelSlim [14], DIGIT [15], DTac [16], etc., can reconstruct the 3D geometry of the contact object surface with high precision. Some of these, like Gelsight wedge [17], and UVTac [18] can also sense the pressure and shear applied on the sensors during the contact. Besides, relevant researches also indicate that the pressure, shear, and location information can be inferred simultaneously [19], [20].

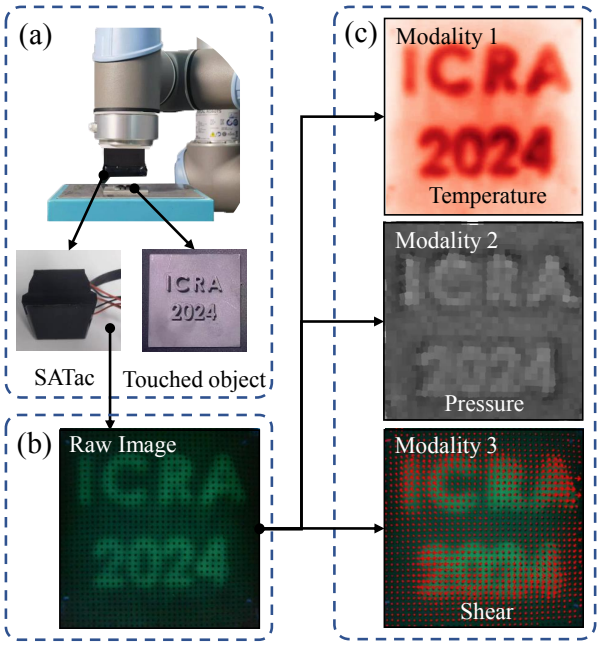

Fig. 1. (a) SATac, the touched object, and the robot arm equipped with SATac exploring the environment. (b) The raw image captured by the camera inside SATac. (c) The three modalities including temperature, pressure, and shear decoupled from the raw image.

Tactile perception of humans is inherently multi-modal: beyond deformation and force, elements such as vibration, humidity, and temperature play crucial roles in tactile sensation. Multi-modal information can also be vital for robotic robotic tactile sensing, which has received considerable attention [21]–[23]. Inspired by the mechanism of human skin, authors in [1] have proposed a flexible multi-modal tactile sensor. The sensor perceives contact pressure and vibration information from the sensor's integrated electrode and microphone array based on techniques of electrical

* The authors contributed equally to this work.

This work was supported by Shenzhen Ubiquitous Data Enabling Key Lab under Grant No. ZDSYS20220527171406015, by Guangdong Innovative and Entrepreneurial Research Team Program (2021ZT09L197), by Shenzhen Science and Technology Program (JCYJ20220530143013030), by Tsinghua Shenzhen International Graduate School-Shenzhen Pengrui Young Faculty Program of Shenzhen Pengrui Foundation (No. SZPR2023005). We also acknowledge the support from the Tsinghua Shenzhen International Graduate School-Shenzhen Pengrui Endowed Professorship Scheme of Shenzhen Pengrui Foundation. *(Z. Song and R. Yu contributed equally to this work. Corresponding author: W. Ding.)*

Z. Song, R. Yu, X. Zhang, K. Su, X.-P. Zhang, and W. Ding are with Shenzhen International Graduate School, Tsinghua University, China. E-mail:{song-zw20,yur23,x-zhang23,sujh21,msl22}@mails.tsinghua.edu.cn, {xiaoping.zhang,ding.wenbo}@sz.tsinghua.edu.cn.

D. Peng is with Shenzhen University, China. E-mail:{pengdengfeng}@szu.edu.cn

X.-P. Zhang and W. Ding are also with RISC-V International Open Source Laboratory, Shenzhen, China, 518055.

X.-P. Zhang is also with the Department of Electrical, Computer, and Biomedical Engineering, Ryerson University, Toronto, ON M5B 2K3, Canada.

impedance tomography and photo-acoustic tomography.

As a major component of tactile perception, temperature sensing is important for humans. This capability can also allow robots to interact better with the external environment. Temperature sensing helps robots avoid potential harm. For instance, a robot equipped with temperature sensors can detect and avoid overheated machinery, preventing damage to its components or objects. Since different materials react differently to temperature changes, robots can adjust their grip strength and handling strategy to accommodate the material's current state by sensing temperature. This significantly enhances the manipulation ability of robots in complex environments. Recognizing the pivotal role of temperature sensing for robotics, researchers have actively developed advanced sensors to refine this capability. Authors in [24] proposed a 5×5 sensing array based on a Ni-NiO-Ni structure, especially for temperature perception. This sensor exhibits excellent negative temperature coefficient characteristics within the range of 20 °C to 70 °C, providing high sensitivity for temperature sensing. There also exists research about multi-modal temperature sensing. A quadruple tactile sensor has been proposed in [25], equipped with two pairs of sensing elements arranged on either side of a layer of sponge material, which can be used to determine the pressure applied on the sensor and the temperature of the contacted object. However, this method does not achieve high-resolution spatial perception [26] concurrently with temperature sensing. This raises a natural question: Is it feasible to develop a tactile sensor for robotic perception that seamlessly integrates temperature sensing with high spatial resolution?

This study introduces a high-resolution, vision-based multi-modal tactile sensor named SATac (as shown in Fig. 1) that can concurrently detect temperature, pressure, and shear. It utilizes Strontium Aluminate (SA) [27], [28], a type of thermoluminescence material. The core sensing component of SATac is the SA film and a method for preparing SA film is also proposed. By laser-cutting small circular holes and filling them with black silicone, the SA film achieves nearly unobstructed temperature distribution, aided by guided filtering. Additionally, pressure distribution and shear force distribution during object contact are sensed by tracking changes in Voronoi polygon areas and centroid displacements. We conducted experiments on objects with complex shapes to demonstrate SATac's excellent performance in multi-modal tactile perception. The main contributions of this paper can be summarized as follows:

- Using SA as the functional material, we introduced SATac, a high-resolution multi-modal tactile sensor capable of concurrently detecting temperature, pressure, and shear.
- SATac can continuously perceive multi-modal data on temperature, pressure, and shear with minimal interference. This capability is achieved through the design of an UltraViolet C radiation (UVC) light field, combined with a layered arrangement of SA film markers and complementary data processing algorithms.
- The perceptual performance of SATac in its three modalities has been characterized, and the exploration and discussion of SATac's applications in different scenarios have been conducted.

The rest of this paper is organized as follows. We present the design and fabrication of SATac in Section II. Section III introduces the methodology of feature extraction. Then we evaluate the performance of SATac with a series of experiments and explore its potential application scenarios in Section IV. The whole paper ends with the discussion and conclusion in Section V.

II. Sensor Design and Fabrication

In this section, we aim to elucidate the design and fabrication process of SATac.

A. SA Material

SA material endows SATac with the capability of perceiving temperature. As a fluorescent material with thermoluminescent properties, SA emits visible light with a wavelength near 520 nm when thermally excited, and the luminescence intensity is temperature-dependent. Typically, within the temperature range of 50 °C to 180 °C, the luminescence intensity increases as the temperature rises. Once the temperature surpasses 180 °C, the luminescence intensity gradually diminishes. With these properties, SA can be used in vision-based tactile sensing, aiding in detecting a relatively broad range of temperature distributions.

The persistent thermoluminescence of SA necessitates external charging, which is determined by its underlying mechanism. When thermally excited, electrons in traps undergo a transition from low to high energy levels. They then revert to lower energy levels, emitting photons in the process. After releasing photons, electrons often transition to even lower energy levels than the initial state, which means that the required excitation temperature for the next cycle becomes higher. This makes thermoluminescent properties non-reusable over multiple cycles, and the relationship between temperature and luminescence intensity can change with the number of thermal excitation and the excitation temperature. To maintain SA at a consistent initial energy level for successive thermoluminescence events, we use ultraviolet light for charging. This procedural step guarantees that SA consistently reverts to a stable luminosity level following each thermoluminescent event, ensuring its readiness for subsequent excitation.

B. SA Film

The SA film is made of silicone and SA powder for temperature perception. SA in its powdered form is widely used and cost-effective. When combined with silicone at a precise mass ratio, it neither disrupts the solidification process of the silicone nor compromises its elasticity. This composite, referred to as SA-Silicone, also demonstrates thermoluminescent characteristics, with luminescence intensity proportionally increasing as the temperature rises. On the SA film, there is a black marker array, which neither emits light nor transmits visible light. The diameter of each

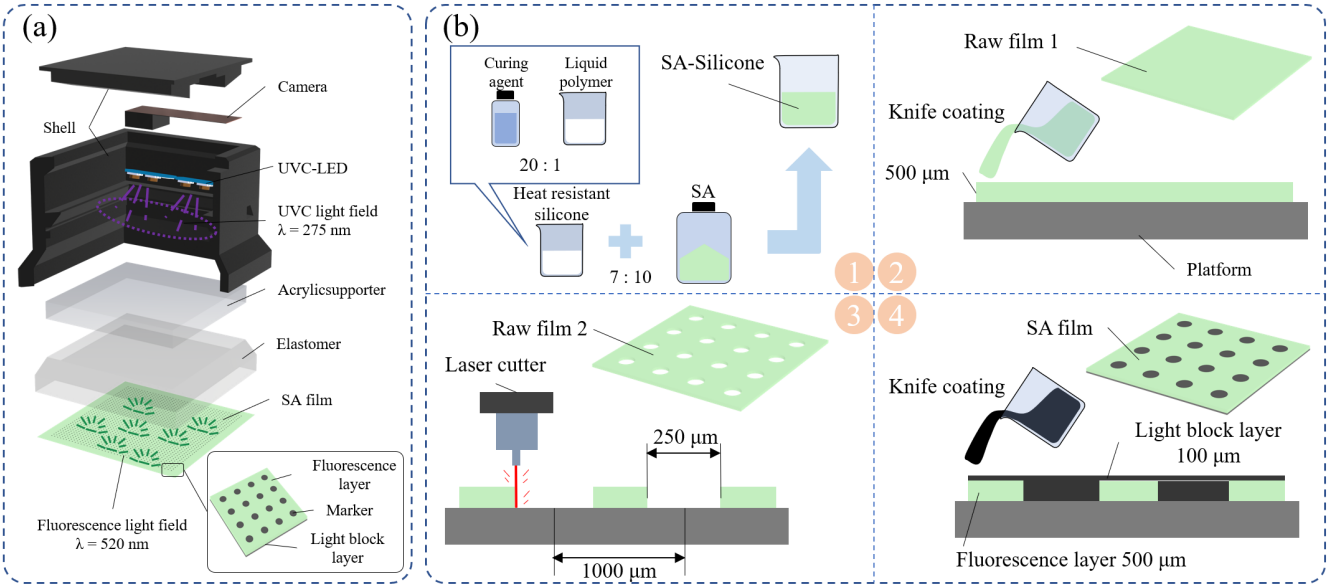

Fig. 2. Design and fabrication process of SATac: (a) The exploded view of SATac. (b) The SA film four steps to fabrication: step 1, mix the heat-resistant silicone with powdered SA to make the SA-Silicone; step 2, fabricate Raw film 1 with knife coating; step 3, fabricate Raw film 2 using laser cutting on Raw film 1; step 4, fabricate the SA film with knife coating filling the black silicone in holds.

marker is 0.25 mm and the distance between two adjacent markers is 1 mm as shown in Fig. 2(a).

The whole process of SA film fabrication is illustrated in Fig. 2(b). First, the SA powder, characterized by a particle diameter of 100 nm, is thoroughly mixed with silicone in a mass ratio of 7:10. The mixture is subsequently placed in a negative pressure environment for 15 min to eliminate air bubbles trapped within the silicone. Second, the mixture is evenly scraped onto a flat glass substrate, forming a layer with a thickness of 500 um using knife coating. After placement in a 60 °C environment for approximately 1 hour, the mixture is solidified into Raw film 1 in step 2 of Fig. 2(b). Third, accurate incisions are performed on Raw film 1 using a laser emitting at a wavelength of 10400 nm, resulting in dimensions of 50×50 mm^2 in the form of a square. Within this square region, a 40×40 array of circular perforations is precisely crafted using laser cutting. Each circular aperture has a diameter of 0.25 mm, with a 1 mm spacing between adjacent apertures. Finally, silicone mixed with black pigment, which can block visible light efficiently, is uniformly applied onto the Raw film 2, ensuring the complete filling of the circular holes with the pigmented silicone. Upon the curing of the black silicone, the fabrication process of SA film is completed.

C. Dual-light Field

In Fig. 2(a), we present the SATac design that incorporates a dual-light field: the UVC light field and the fluorescence field. This innovative design allows the SA to revert to its original brightness post-thermoluminescence. Moreover, it equips SATac with enhanced sensing capabilities extending beyond mere temperature perception, encompassing pressure and shear force sensing modalities. As previously mentioned, the UVC light field, with a wavelength of 275 nm, is employed for charging the SA film. Notably, this wavelength is beyond the capture range of standard RGB cameras. On the other hand, the SA film emits a fluorescence field with a wavelength of 520 nm. This fluorescence serves as a backdrop, enabling clear detection of marker positions on the SA film.

D. Overall Sensor Architecture

SATac measures 50 mm in length, 50 mm in width, and 30 mm in height. The complete architecture of the SATac sensor is depicted in Fig. 2. Apart from the SA film that has been introduced, the remaining parts of SATac consist of an outer shell, a camera, a set of UVC-LEDs, a transparent acrylic support, and a polydimethylsiloxane (PDMS) transparent elastomer.

The outer shell is used for protection and to prevent external light from affecting the inside light fields. The camera has a field of view of 105 degrees and a frame rate of 60 FPS and the main optical axis of the camera intersects the center of the SA film and aligns perpendicular to the SA film. 4 UVC-LEDs are placed around the main optical axis of the camera. Each UVC-LED operates at a voltage of 4.7 V, with a total power consumption of 0.5 W. The transparent acrylic support is used to prevent overall deformation of the elastomer, ensuring sufficient contact with objects during the touching. The PDMS elastomer, prepared by mixing liquid polymer and curing agent at a 20:1 ratio, ensures congruent deformation with the SA film. The SA film is firmly bonded to the elastomer using this PDMS mixture. The integration of a transparent elastomer with acrylic support allows the camera to distinctly capture variations in brightness and the movement of markers. Additionally, the transparent PDMS

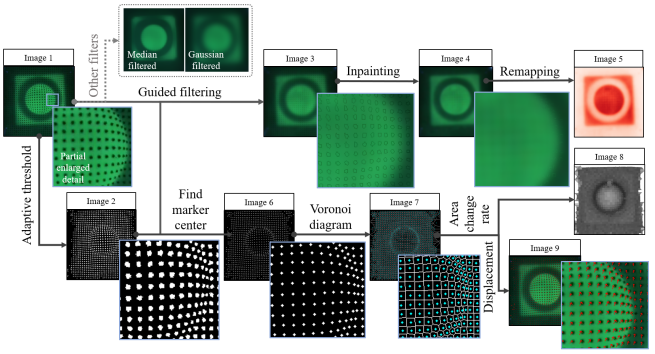

Fig. 3. The complete working flow of inferring temperature (Image 5), pressure (Image 8), and shear (Image 9) from the raw image (Image 1). Temperature information is extracted with methods including guided filtering, inpainting, and remapping. Marker contouring detection and the Voronoi diagram algorithm are used for processing pressure and shear, which are calculated by area change rate and marker displacement respectively.

elastomer and acrylic support permit the transmission of UVC-light, enabling it to irradiate the SA film for energy provision.

III. Feature Extraction

This section introduced the details of inferring the critical features for sensing the temperature distribution, pressure distribution, and shear distribution. All the image processes are achieved using OpenCV [29].

A. Temperature

The thermoluminescence properties of SA indicate that the temperature of a contacted object influences the peak brightness of the SA film. Consequently, the brightness peak extracted from an image can depict the SA film's temperature distribution. The black marker array, being non-luminous and opaque, does not reflect temperature-induced brightness changes, leading to an incomplete temperature representation in Image 1 of Fig. 3. Image 2, derived by applying an adaptive threshold to Image 1, displays all marker contours. These contours guide the guided filtering [30], [31] of Image 1, effectively eliminating the black markers without compromising high-frequency details. Post-filtering, residual contour outlines remain, but a subsequent inpainting operation removes them, as evident in Image 4. This method preserves the SA material's temperature information and fills marker positions by referencing adjacent pixel brightness, yielding a temperature distribution free from market disruptions.

To further explain the reason for using a guided filter, we compare its filtered image with the Gaussian filter and median filter results as shown in Fig. 3. Although these two filters remove the markers successfully, excessive smoothing exists outside the markers. Comparing Image 1 and Image 4, the combination of guided filtering and impainting realizes both mitigate the influence of markers and prevent the image from distortion. This shows the effectiveness of our proposed method.

B. Pressure and Shear

The estimation of pressure and shear is achieved by analyzing the displacement of markers. In Fig. 3, Image 2 contains the contour information of the markers, after finding and detecting the marker positions, the centers of each marker are located in Image 6. With these contour centers, the Voronoi diagram of each center can be figured out, which is presented in Image 7.

For pressure distribution, the pressure at the location of each center is presented as the area change ratio of the corresponding Voronoi diagram. In Fig. 3, Image 8 is the remapping results from the area change rate to the brightness of the gray image.

For shear distribution, the shear at the location of each center is presented as the displacement in the image, where the displacement is defined as the difference between the position in the current frame and the position in the original frame. The tracking displacement of all the markers is visualized in Image 9 of Fig. 3, which is considered as the shear distribution.

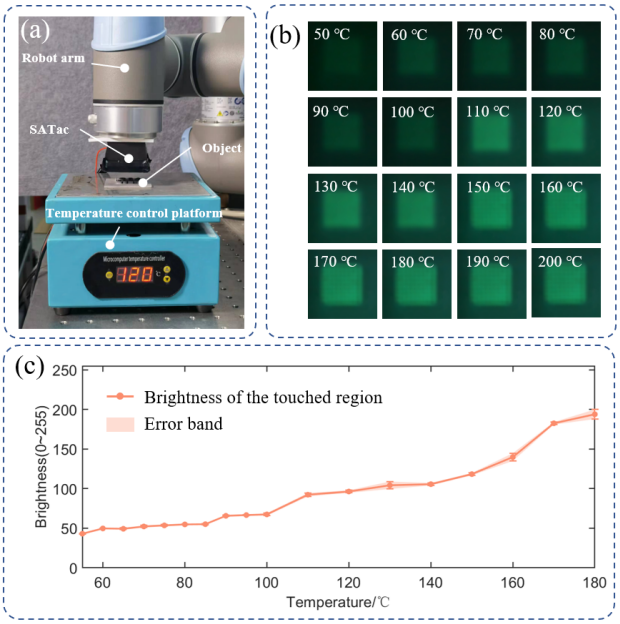

Fig. 4. Characterization Experiment of Temperature Sensing. (a) Experimental setup for characterizing the performance of SATac in temperature sensing. (b) Experimental data for SATac's contact temperature when in contact with objects ranging from 50°C to 200°C. It can be observed that brightness continuously increases from 50°C to 180°C. (c) The relation between brightness and temperature in SATac working range (50°C to 180°C).

IV. Experiments

A. Characterization

A series of experiments have been conducted to verify the performance of SATac, that is the relationship between brightness and three different modalities (temperature, pressure, and sheer).

1) Temperature: In the experiment characterizing the perception of the temperature distribution, SATac is firmly mounted on the end-effector of the UR5 robot arm, as shown in Fig. 4(a). A metal cube with a 10 mm side length is placed at the center of a temperature-controlled platform. The surface temperature is controlled to increase from 50 °C to 200 °C with a 5 °C step. At each temperature value, the robot arm drives SATac to move vertically downward from a distance of 25 mm to the platform at a speed of 20 mm/s, moving a total of 16 mm. After reaching the target position, the cube is in sufficient contact with SATac, and the robot arm maintains static for 5s before returning to the starting point. Fig. 4(b) shows some selected visualization results of the temperature distribution. It can be observed that the brightness gradually increases from 50 °C to 180 °C, and a decrease in brightness occurs after 180 °C. After repeating this experiment five times, we obtained the statistical results shown in Fig. 4(c). In the results of multiple trials, it is evident that the brightness steadily increases with the rise in temperature between 50 °C and 180 °C. The narrow error band indicates the stable performance of SATac in temperature perception.

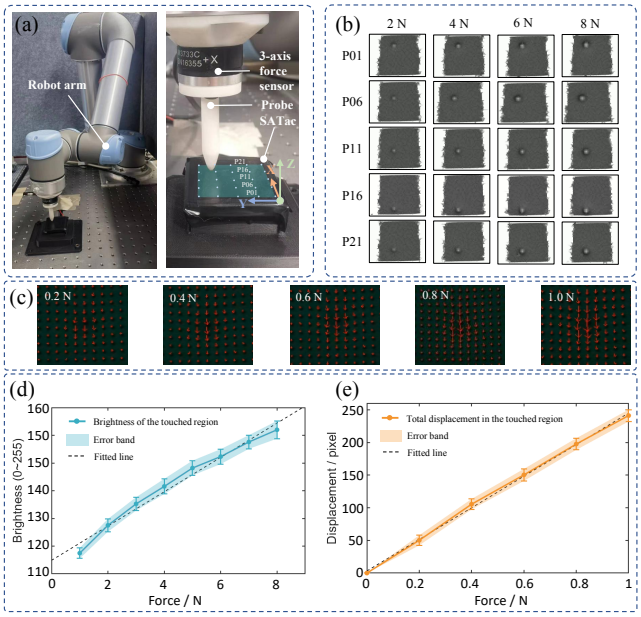

Fig. 5. Characterization experiment of SATac pressure and shear sensing. (a) Experimental setup. (b) Experimental data for applying positive pressures of 2 N, 4 N, 6 N, and 8 N at pressing positions P1, P6, P11, P16, and P21. (c) Experimental data for applying shear of 0.2 N, 0.4 N, 0.6 N, 0.8 N, and 1.0 N. (d) The linear relationship between the brightness and the applied pressure. (e) The linear relationship between the marker displacement and the applied shear force.

2) Pressure and Shear: In the characterization experiment of pressure and Shear perception, the UR5 robot arm and a 6-axis force/Torque sensor (M3733C Sunrise Instruments) are used to standardize contact force and location. As shown in Fig. 5(a), SATac was firmly secured to a flat optical platform via an adapter plate to guarantee that SATac is parallel to the optical platform. A 6-axis force sensor was

Fig. 6. SATac touches different objects for testing their properties and obtains corresponding temperature distribution (80 °C, 120 °C, and 160 °C) and pressure distribution (2 N and 5 N).

mounted on the robot arm, which could provide real-time force measurements along the X, Y, and Z directions shown in Fig. 5(a). A conical probe was attached to the other end of the 6-axis force sensor. Considering that the sensing range of the sensor is 45×45 mm^2, a square region with a size of 35×35 mm^2 is selected in the center of the SATac's sensing region, and 25 sampling points are figured out on the region in Fig. 5(a).

In the pressure characterization study, a robot arm guides a probe to apply forces from 1 N to 8 N with a step of 1 N at 25 sample positions. The probe initially positioned 20 mm above the sensor center, descends at 5 mm/s toward the target. For each force increment (from 1 N to 8 N), once the 6-axis force sensor indicates the desired force, the arm halts, maintaining pressure for 5s, then continues descending. This is repeated until the force reaches 8 N. Subsequently, the probe returns to the 1 N position and moves along the X direction. When the force output in the X direction hits increments from 0.2 N to 1.0 N, the same 5s pause procedure is implemented. The process concludes by returning the probe to its initial position, and this cycle is performed across all 25 sampling positions.

Some selected pressure distributions output by SATac are shown in Fig. 5(b). It can be observed from the result that greater forces are exerted at varying positions, while increased brightness coincides with these locations in the remapped pressure distribution. Fig. 5(c) shows some selected shear distributions from SATac. The relationship between pressure and brightness is presented in Fig. 5(d). The relationship between shear and the cumulative displacement of all markers is presented in Fig. 5(e). For both pressure and shear experiments, we conduct multiple repeated experiments to calculate the corresponding error bars and error bands. The results reveal a strong linear correlation between brightness and both pressure and shear, with relatively small errors.

B. Application

SATac possesses the capability to concurrently acquire multi-modal information with exceptional resolution. Ex-

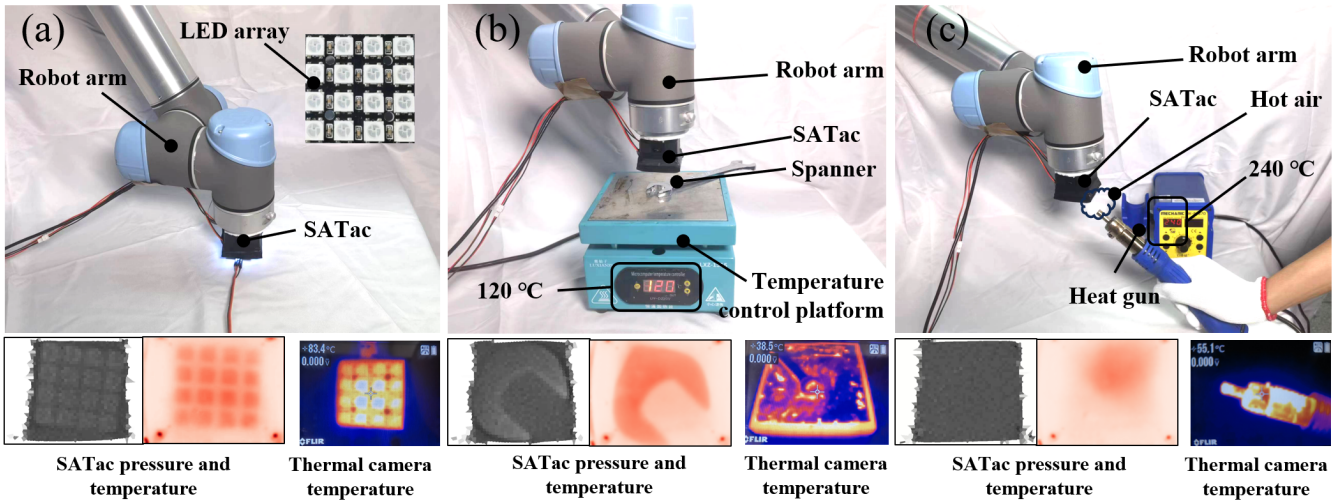

Fig. 7. Performance of SATac in Four Scenarios. (a) SATac touches a working LED array circuit board. (b) SATac touches a metallic spanner heated by the temperature control platform. The temperature is set to be 120°C. (c) In a non-contact situation, SATac senses a high-temperature gas from a heat gun. The temperature of the gas is set to be 240°C.

periments were conducted by affixing SATac to the end of a robotic arm, enabling it to sense objects of varying complex shapes. Fig. 6 illustrates the perception results under varying temperature and contact pressure conditions. These results demonstrate a commendable ability to acquire multi-modal information, as evidenced by its robust performance in diverse experimental conditions.

In certain scenarios, the commonly used high-resolution temperature measurement method can not accurately measure the temperature of target objects, and SATac offers a solution to this challenge. We have conducted a series of experiments to compare the performance between SATac and a high-performance thermal camera (Guide PS400). As shown in Fig. 7(a), we simulate one possible scenario where an illuminated LED array with each LED is at 80 °C. The thermal camera reveals a central LED cluster with a higher temperature than its periphery, which is not in line with the actual situation. This is caused by interference between different lights. Similarly, in Fig. 7(b) and Fig. 7(c), the thermal camera struggles to measure the temperature accurately due to metal reflection and the passage of infrared light through hot air, respectively. SATac shows better performances when dealing with those situations. Additionally, sensing results of SATac in Fig. 7(a) and (b) also show multi-modal ability by measuring pressure distribution. Considering the result of Fig. 7(c), although there is no remarkable deformation on the sensor's surface, multi-modal ability enables SATac to sense the hot air, which can be hardly detected by conventional vision-based sensors.

V. Discussions and Conclusion

This paper introduces SATac, a high-resolution multi-modal vision-based tactile sensor based on the thermoluminescence material. SATac is capable of simultaneously perceiving temperature distribution, pressure distribution, and shear force distribution of the contacted object. Moreover, due to its high resolution, it can also discern object shapes and spatial positions of contact areas. The core sensing component of SATac is the SA film and a method for preparing SA film is proposed. By laser-cutting small circular holes and filling them with black silicone, the SA film achieves nearly unobstructed temperature distribution, aided by guided filtering. Additionally, pressure distribution and shear force distribution during object contact are sensed by tracking Voronoi polygon area changes and centroid displacements. We conducted experiments on objects with complex shapes to demonstrate SATac's excellent performance in multi-modal tactile perception.

TABLE I

Comparison of the Vision-Based Tactile Sensors

Sensor	Size (mm)	Sensing field (mm^2)	Camera resolution	Modality
DIGIT [15]	20×27×18	19×16	640×480	3D deformation
DTact [16]	45×45×47	24×24	800×600	3D deformation
DotView [32]	25.5×47×14.4	8×8	192×192	pressure and shear
DelTact [33]	39×60×30	36×34	1280×720	3D deformation, pressure and shear
TacRot [34]	42×84×45	N/A	800×600	3D deformation, pressure and shear
SATac (Ours)	**50×50×30**	**40×40**	**640×480**	**temperature, pressure and shear**

Compared to previous classical multi-modal tactile sensing approaches as shown in Table I, SATac offers the advantage of perceiving temperature, pressure, and shear force simultaneously while also providing information about object shape and contact location. It encompasses a broader range of sensing modalities and boasts a considerable sensing area and sampling frequency.

The main limitation of SATac is the limited temperature sensing range between 50 °C to 180 °C. In the future, we can explore the possibility of customizing the temperature sensing range by introducing specific ion doping to the SA material, allowing it to cover a broader temperature range.

REFERENCES

[1] K. Park, H. Yuk, M. Yang, J. Cho, H. Lee, and J. Kim, "A biomimetic elastomeric robot skin using electrical impedance and acoustic tomography for tactile sensing," *Science Robotics*, vol. 7, no. 67, p. eabm7187, 2022.

[2] S. Dong, D. K. Jha, D. Romeres, S. Kim, D. Nikovski, and A. Rodriguez, "Tactile-RL for insertion: Generalization to objects of unknown geometry," in *IEEE International Conference on Robotics and Automation (ICRA)*, Xi'an, China, 2021, pp. 6437–6443.

[3] S. Pai, T. Chen, M. Tippur, E. Adelson, A. Gupta, and P. Agrawal, "TactoFind: A tactile only system for object retrieval," *arXiv preprint arXiv:2303.13482*, 2023.

[4] Z. Song, J. Yin, Z. Wang, C. Lu, Z. Yang, Z. Zhao, Z. Lin, J. Wang, C. Wu, J. Cheng *et al.*, "A flexible triboelectric tactile sensor for simultaneous material and texture recognition," *Nano Energy*, vol. 93, p. 106798, 2022.

[5] M. K. Johnson and E. H. Adelson, "Retrographic sensing for the measurement of surface texture and shape," in *IEEE/CVF Conference on Computer Vision and Pattern Recognition (CVPR)*, FL, USA, 2009, pp. 1070–1077.

[6] T. Wang, H.-J. Joo, S. Song, W. Hu, C. Keplinger, and M. Sitti, "A versatile jellyfish-like robotic platform for effective underwater propulsion and manipulation," *Science Advances*, vol. 9, no. 15, p. eadg0292, 2023.

[7] H. Yin, A. Varava, and D. Kragic, "Modeling, learning, perception, and control methods for deformable object manipulation," *Science Robotics*, vol. 6, no. 54, p. eabd8803, 2021.

[8] W. G. Bircher, A. S. Morgan, and A. M. Dollar, "Complex manipulation with a simple robotic hand through contact breaking and caging," *Science Robotics*, vol. 6, no. 54, p. eabd2666, 2021.

[9] H. Sun, K. J. Kuchenbecker, and G. Martius, "A soft thumb-sized vision-based sensor with accurate all-round force perception," *Nature Machine Intelligence*, vol. 4, no. 2, pp. 135–145, 2022.

[10] J. Qu, B. Mao, Z. Li, Y. Xu, K. Zhou, X. Cao, Q. Fan, M. Xu, B. Liang, H. Liu *et al.*, "Recent progress in advanced tactile sensing technologies for soft grippers," *Advanced Functional Materials*, p. 2306249, 2023.

[11] A. C. Abad and A. Ranasinghe, "Visuotactile sensors with emphasis on GelSight sensor: A review," *IEEE Sensors Journal*, vol. 20, no. 14, pp. 7628–7638, 2020.

[12] S. Zhang, Z. Chen, Y. Gao, W. Wan, J. Shan, H. Xue, F. Sun, Y. Yang, and B. Fang, "Hardware technology of vision-based tactile sensor: A review," *IEEE Sensors Journal*, 2022.

[13] S. Li, H. Yu, W. Ding, H. Liu, L. Ye, C. Xia, X. Wang, and X.-P. Zhang, "Visual–tactile fusion for transparent object grasping in complex backgrounds," *IEEE Transactions on Robotics*, 2023.

[14] I. H. Taylor, S. Dong, and A. Rodriguez, "GelSlim 3.0: High-resolution measurement of shape, force and slip in a compact tactile-sensing finger," in *International Conference on Robotics and Automation (ICRA)*, PA, USA, 2022, pp. 10 781–10 787.

[15] M. Lambeta, P.-W. Chou, S. Tian, B. Yang, B. Maloon, V. R. Most, D. Stroud, R. Santos, A. Byagowi, G. Kammerer *et al.*, "DIGIT: A novel design for a low-cost compact high-resolution tactile sensor with application to in-hand manipulation," *IEEE Robotics and Automation Letters*, vol. 5, no. 3, pp. 3838–3845, 2020.

[16] C. Lin, Z. Lin, S. Wang, and H. Xu, "DTact: A vision-based tactile sensor that measures high-resolution 3D geometry directly from darkness," in *IEEE International Conference on Robotics and Automation (ICRA)*, London, United Kingdom, 2023, pp. 10 359–10 366.

[17] S. Wang, Y. She, B. Romero, and E. Adelson, "GelSight Wedge: Measuring high-resolution 3d contact geometry with a compact robot finger," in *IEEE International Conference on Robotics and Automation (ICRA)*, Xi'an, China, 2021, pp. 6468–6475.

[18] W. Kim, W. D. Kim, J.-J. Kim, C.-H. Kim, and J. Kim, "UVtac: Switchable UV marker-based tactile sensing finger for effective force estimation and object localization," *IEEE Robotics and Automation Letters*, vol. 7, no. 3, pp. 6036–6043, 2022.

[19] L. Cramphorn, J. Lloyd, and N. F. Lepora, "Voronoi features for tactile sensing: Direct inference of pressure, shear, and contact locations," in *IEEE International Conference on Robotics and Automation (ICRA)*, QLD, Australia, 2018, pp. 2752–2757.

[20] N. F. Lepora, "Soft biomimetic optical tactile sensing with the TacTip: A review," *IEEE Sensors Journal*, vol. 21, no. 19, pp. 21 131–21 143, 2021.

[21] Y.-E. Shin, Y.-J. Park, S. K. Ghosh, Y. Lee, J. Park, and H. Ko, "Ultrasensitive multimodal tactile sensors with skin-inspired microstructures through localized ferroelectric polarization," *Advanced Science*, vol. 9, no. 9, p. 2105423, 2022.

[22] P. Mittendorfer and G. Cheng, "Humanoid multimodal tactile-sensing modules," *IEEE Transactions on robotics*, vol. 27, no. 3, pp. 401–410, 2011.

[23] W. Choi, I. Yun, J. Jeung, Y. S. Park, S. Cho, D. W. Kim, I. S. Kang, Y. Chung, and U. Jeong, "Stretchable triboelectric multimodal tactile interface simultaneously recognizing various dynamic body motions," *Nano Energy*, vol. 56, pp. 347–356, 2019.

[24] J. Shin, B. Jeong, J. Kim, V. B. Nam, Y. Yoon, J. Jung, S. Hong, H. Lee, H. Eom, J. Yeo *et al.*, "Sensitive wearable temperature sensor with seamless monolithic integration," *Advanced Materials*, vol. 32, no. 2, p. 1905527, 2020.

[25] G. Li, S. Liu, L. Wang, and R. Zhu, "Skin-inspired quadruple tactile sensors integrated on a robot hand enable object recognition," *Science Robotics*, vol. 5, no. 49, p. eabc8134, 2020.

[26] N. F. Lepora, Y. Lin, B. Money-Coomes, and J. Lloyd, "Digitac: A digit-tactip hybrid tactile sensor for comparing low-cost high-resolution robot touch," *IEEE Robotics and Automation Letters*, vol. 7, no. 4, pp. 9382–9388, 2022.

[27] Z. Huang, B. Chen, B. Ren, D. Tu, Z. Wang, C. Wang, Y. Zheng, X. Li, D. Wang, Z. Ren *et al.*, "Smart mechanoluminescent phosphors: A review of strontium-aluminate-based materials, properties, and their advanced application technologies," *Advanced Science*, vol. 10, no. 3, p. 2204925, 2023.

[28] X. Liu, L. Zhang, D. Wang, D. Wang, H. Shen, H. Wu, H. Wu, G. Pan, Z. Hao, F. Liu *et al.*, "Liquid nitrogen temperature mechanoluminescence and persistent luminescence," *Advanced Functional Materials*, p. 2305275, 2023.

[29] O. Team, *Open Source Computer Vision Library*, 2023. [Online]. Available: https://opencv.org/

[30] K. He, J. Sun, and X. Tang, "Guided image filtering," *IEEE Transactions on Pattern Analysis and Machine Intelligence*, vol. 35, no. 6, pp. 1397–1409, 2012.

[31] S. Mao, M. Ji, B. Wang, Q. Dai, and L. Fang, "Surface material perception through multimodal learning," *IEEE Journal of Selected Topics in Signal Processing*, vol. 16, no. 4, pp. 843–853, 2022.

[32] H. Zheng, Y. Jin, H. Wang, and P. Zhao, "DotView: A low-cost compact tactile sensor for pressure, shear, and torsion estimation," *IEEE Robotics and Automation Letters*, vol. 8, no. 2, pp. 880–887, 2023.

[33] G. Zhang, Y. Du, H. Yu, and M. Y. Wang, "DelTact: A vision-based tactile sensor using a dense color pattern," *IEEE Robotics and Automation Letters*, vol. 7, no. 4, pp. 10 778–10 785, 2022.

[34] W. Zhang, C. Xia, X. Zhu, H. Liu, and B. Liang, "TacRot: A parallel-jaw gripper with rotatable tactile sensors for in-hand manipulation," in *IEEE International Conference on Systems, Man, and Cybernetics (SMC)*, Prague, Czech Republic, 2022, pp. 423–429.